

On microscopic compositional and electrostatic properties of grain boundaries in polycrystalline Cu In $1 - x$ Ga x Se 2

M. J. Hetzer, Y. M. Strzhemechny, M. Gao, S. Goss, M. A. Contreras, A. Zunger, and L. J. Brillson

Citation: *Journal of Vacuum Science & Technology B* **24**, 1739 (2006); doi: 10.1116/1.2209995

View online: <http://dx.doi.org/10.1116/1.2209995>

View Table of Contents: <http://scitation.aip.org/content/avs/journal/jvstb/24/4?ver=pdfcov>

Published by the AVS: Science & Technology of Materials, Interfaces, and Processing

Articles you may be interested in

[Physics of grain boundaries in polycrystalline photovoltaic semiconductors](#)

J. Appl. Phys. **117**, 112807 (2015); 10.1063/1.4913833

[Symmetry dependent optoelectronic properties of grain boundaries in polycrystalline Cu\(In,Ga\)Se₂ thin films](#)

J. Appl. Phys. **115**, 023514 (2014); 10.1063/1.4861149

[Evaluation of Kelvin probe force microscopy for imaging grain boundaries in chalcopyrite thin films](#)


Appl. Phys. Lett. **89**, 113120 (2006); 10.1063/1.2354474




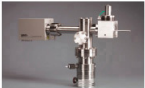
[Direct observation of copper depletion and potential changes at copper indium gallium diselenide grain boundaries](#)

Appl. Phys. Lett. **86**, 162105 (2005); 10.1063/1.1906331

[Local built-in potential on grain boundary of Cu\(In,Ga\)Se₂ thin films](#)

Appl. Phys. Lett. **84**, 3477 (2004); 10.1063/1.1737796


Instruments for Advanced Science

<p>Contact Hiden Analytical for further details: W www.HidenAnalytical.com E info@hiden.co.uk</p> <p>CLICK TO VIEW our product catalogue</p>	 <p>Gas Analysis</p> <ul style="list-style-type: none"> › dynamic measurement of reaction gas streams › catalysis and thermal analysis › molecular beam studies › dissolved species probes › fermentation, environmental and ecological studies 	 <p>Surface Science</p> <ul style="list-style-type: none"> › UHV TPD › SIMS › end point detection in ion beam etch › elemental imaging - surface mapping 	 <p>Plasma Diagnostics</p> <ul style="list-style-type: none"> › plasma source characterization › etch and deposition process reaction › kinetic studies › analysis of neutral and radical species 	 <p>Vacuum Analysis</p> <ul style="list-style-type: none"> › partial pressure measurement and control of process gases › reactive sputter process control › vacuum diagnostics › vacuum coating process monitoring
---	--	--	--	--

On microscopic compositional and electrostatic properties of grain boundaries in polycrystalline $\text{CuIn}_{1-x}\text{Ga}_x\text{Se}_2$

M. J. Hetzer^{a)}

Department of Physics, The Ohio State University, Columbus, Ohio 43210

Y. M. Strzhemechny

Department of Physics and Astronomy, Texas Christian University, Fort Worth, TX 76129

M. Gao and S. Goss

Department of Electrical and Computer Engineering, The Ohio State University, Columbus, Ohio 43210

M. A. Contreras and A. Zunger

National Renewable Energy Laboratory, Golden, Colorado 80401

L. J. Brillson

Department of Physics, The Ohio State University, Columbus, Ohio 43210, Center for Materials Research, The Ohio State University, Columbus, Ohio 43210, and Department of Electrical and Computer Engineering, The Ohio State University, Columbus, Ohio 43210

(Received 23 November 2005; accepted 11 May 2006; published 28 June 2006)

We report on the microscopic characteristics of polycrystalline $\text{CuIn}_{1-x}\text{Ga}_x\text{Se}_2$ thin films probed with Auger electron spectroscopy, cathodoluminescence spectroscopy, secondary ion mass spectrometry, and work function measurements. Confirming theory, we find a substantial reduction in Cu content from grain interior to boundary and a *p*-type potential barrier that acts to reduce hole recombination. Such compositional and electrostatic variations between grain boundaries and grain interiors in $\text{CuIn}_{1-x}\text{Ga}_x\text{Se}_2$ solar cell absorber layers may improve the overall photovoltaic efficiency. The high degree of intergranular inhomogeneity emphasizes the importance of detailed grain-by-grain analysis. These results show that careful specimen preparation and ultrahigh vacuum conditions, coupled with nanoscale instrumental resolution, are pivotal for such analysis. © 2006 American Vacuum Society. [DOI: 10.1116/1.2209995]

I. INTRODUCTION

$\text{CuIn}_{1-x}\text{Ga}_x\text{Se}_2$ (CIGS) is an important photovoltaic material. Notably, record conversion efficiencies of nearly 20% (Ref. 1) are observed for polycrystalline CIGS devices, which outperform their single crystalline counterparts.² This high performance combined with the cheaper polycrystalline technology seems very promising for large area solar cell applications. Several models have been proposed to explain the photovoltaic performance of chalcopyrite polycrystalline material.^{3–8} Unlike the surfaces of III-V materials, which are most stable with a nonpolar termination,⁹ chalcopyrite surfaces tend to terminate with polar facets.¹⁰ Such orientations require a massive (up to 50%) removal of Cu atoms to cancel the otherwise energetically costly electrostatic dipoles. In a recent paper, Persson and Zunger³ viewed the CIGS grain boundary (GB) as a surfacelike dipolar structure. Their calculations predicted that the interface between the stoichiometric grain interior (GI) and the Cu-deficient GB would lower the valence band maximum at the GB by up to 400 meV. Significantly, these electronic changes were shown to produce only charge-neutral band bending, without mobility-reducing charged GB donors. This model emphasizes the existence of charge-neutral vacancies at the GB. Note that charge-neutral vacancies exist also in ordered vacancy compounds which can cause, in principle, band bend-

ing too,^{11,12} but the existence of ordered vacancy phases in device-material CIGS was not demonstrated as yet. This chemically induced (nonelectrostatic) band offset would repel holes from the GB, suppressing recombination with electrons despite an expected large density of recombination centers. The authors have pointed out that such behavior has wider significance for polycrystalline materials in general and could usher in a more extensive range of applications for polycrystalline films. Alternative models deal with *n*-type band bending at GBs and the presence of charged GB donors.⁴ Two such models predict the band bending of both the valence as well as the conduction band. A different view of the GB chemistry was suggested in Refs. 6–8 for CIS samples, in which O atoms are predicted to compensate Se deficiency. Such passivation would improve intergrain electron transport since Se vacancies act as donors. These would create an *n*-type depletion layer that acts as a potential barrier for electronics. Oxygen atoms at Se sites would reduce such donor concentration. In Ref. 13 the authors reported scanning Kelvin probe measurements on CdTe/CdS films, showing that the GBs are depleted. They suggested that this is due to electrostatic band bending created by the positively charged donor Cl-on-Te, following the CdCl_2 treatment. This specialized mechanism is different from the nonelectrostatic band offset discussed earlier in Ref. 3 for ternary (chalcopyrite) systems.

^{a)}Electronic mail: mhetzer@pacific.mps.ohio-state.edu

Given such a variety of proposed models, a set of techniques is needed to probe CIGS stoichiometry and electrostatics with nanoscale sensitivity in order to evaluate the different mechanisms. Numerous studies have been performed on CIGS and related systems addressing grain chemistry and morphology.^{14–17} In our recent paper¹⁸ we reported on the direct measurements of elemental composition of the individual grains and their boundaries. We showed that copper composition at CIGS GBs decreases, sometimes by almost a factor of 2, and that the work function decreases by several hundred meV. In this article, we provide additional results supporting our findings. We investigate chemical composition, potential distribution, and optoelectronic features of GIs and GBs on ultrahigh vacuum (UHV) cleaved CIGS cross-section surfaces. By employing Auger electron spectroscopy (AES), secondary electron threshold (SET) measurements, cathodoluminescence spectroscopy (CLS), and secondary ion mass spectroscopy (SIMS) we confirm the theoretical predictions for the hole barrier at GBs due to Cu deficiency and report on the complex morphological properties of this material.

II. EXPERIMENTAL DETAILS

The samples studied in this work were grown on a soda lime glass substrate with a Mo back contact using a three step process described elsewhere.¹ The layer thicknesses were 1.5–2.0 μm for CIGS and $\sim 0.7 \mu\text{m}$ for Mo. The samples had four different nominal Cu/(In+Ga) ratios of 0.78, 0.85, 0.93, and 0.99, and a Ga/(In+Ga) ratio of 0.30, as determined by inductively coupled plasma spectroscopy. In order to obtain high-quality cleaved cross sections, the following procedure was implemented. First, the glass backside of a sample was thinned by grinding to bring the sample thickness to $\sim 1 \text{ mm}$. The backsides were then notched with a diamond saw to a depth of $\sim 500 \mu\text{m}$. An $\sim 300 \text{ \AA}$ thick Ni layer was deposited on the backside to create an electrical contact to reduce charging due to electron-beam bombardment. The samples were cleaved in vacuum prior to measurement in an ambient pressure of $\sim 10^{-9}$ Torr and then immediately transferred to the main chamber with pressure of $\sim 10^{-10}$ Torr. The *in situ* measurements were performed employing a JEOL 7800F scanning electron microprobe equipped with a hemispherical electron analyzer and Oxford CLS setup (a parabolic mirror coupled with a monochromator and Ge detector).¹⁹ The electron beam parameters used were 5.0 keV, 10.0 nA for the AES measurements, 5.0 keV, 1.0 nA for the SET measurements, and 10.0 keV, 100.0 pA for the CLS measurements. The *e*-beam spot size for these configurations was in the range of 9–43 nm. The SET data was taken on a freshly cleaved surface to minimize changes in the surface potential due to contamination. AES measurements were then performed after this, and the contamination levels were checked prior to data collection.

AES and SET measurements were performed with the incident electron beam at a nominal angle of 45° to the sample surface, with the sample face normal to the hemispherical analyzer. To collect the AES and SET data, the

electron beam was placed at set points crossing one or more GBs and data were acquired from each spot. According to Powell²⁰ Monte Carlo simulations taking into account the effects of backscattered electrons are needed for realistic estimates of the measured area in AES measurements. From such simulation we find an effective area of approximately 100 nm for the lateral spread in our AES measurement, consistent with the results of Ref. 20. Angular variation in the cleaved surface may reduce the lateral resolution of these measurements. Since portions of the cleaved surface are not flat, there may be some spreading of the spot size due to such angular variations. We avoided such effects by limiting our studies to regions that appeared flat in the scanning electron microprobe (SEM) image. The depth of the region probed for the AES and SET measurements was limited to the outermost few monolayers of the sample. The depth probed by the CLS measurement varies with the energy of the incident beam. For 5 keV, this peak excitation depth was approximately 100 nm. We also performed Auger spectral line scans, monitoring AES peak intensity versus position along a line of points.

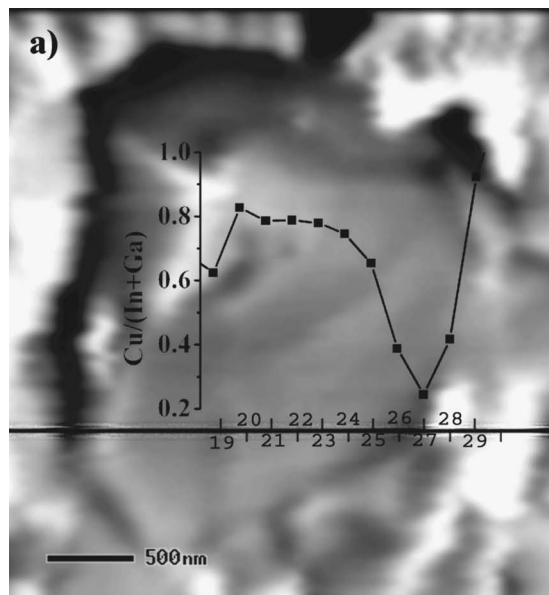
We collected CLS measurements at $T \sim 15 \text{ K}$ with the electron beam normal to the cleaved surface of the sample. The spatial resolution of the CLS measurement is determined both by the energy dependent beam “blooming” as well as any diffusion of minority carriers. The diffusion of carriers can be estimated from the value found in CdS previously²¹ to be in the range of tens of nanometers. SET and AES measurements were performed on a wide array of grain boundaries and grains, including some on the same grain boundaries. However, these were not performed sequentially; SET measurements were all performed before AES scans in order to minimize any effects of surface contamination. Subsequent AES measurements confirmed low contamination levels. The large number of grains and boundaries examined permitted us to identify characteristic AES behavior (smaller set for SET data) despite grain-to-grain variations.

SIMS depth profiles were obtained on a PHI Trift III time-of-flight secondary ion mass spectroscopy (TOF-SIMS) instrument. Data were collected using a 25 keV gallium analysis beam and a 3 keV oxygen sputter beam. For these measurements, the area probed was $25 \times 25 \mu\text{m}^2$. The spatial resolution for these measurements was approximately 150 nm. The uncertainty in the chemical signals is ± 10 counts.

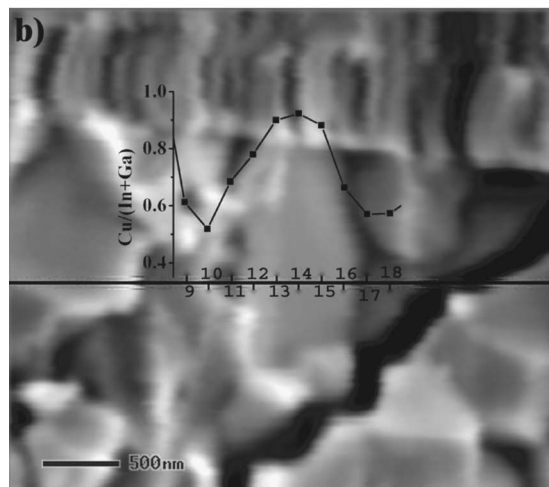
III. RESULTS

A. Auger electron spectroscopy

AES results for all the four sample stoichiometries demonstrate that Cu/(In+Ga) ratios decrease at GBs. Two scans from the sample with nominal Cu/(In+Ga) ratio equal to 0.78 are shown in Fig. 1. We obtained AES elemental percentages from $dN(E)/dE$ peak-to-peak intensities normalized to sensitivity factors provided by the manufacturer for our hemispherical analyzer. These values were then used to calculate the Cu/(In+Ga) ratios at each point. We performed a



(a)



(b)

FIG. 1. (a) AES Cu/(In+Ga) ratio vs position, shown in SEM image. A decrease occurs at the GB (point 27). The data points were taken along the line shown in the figure at the labeled points. The Cu/(In+Ga) ratio at each point is overlaid. (b) AES Cu/(In+Ga) ratio vs position, shown in SEM image. A decrease occurs at the GBs (points 10 and 17). The data points were taken along the line shown in the figure at the labeled points. The Cu/(In+Ga) ratio at each point is overlaid.

statistical analysis for all of the AES data taken. Data points were classified as either GI or GB as determined from the secondary electron (SE) images taken for each scan. Over 100 GBs, with significantly more GI points, were studied and analyzed from the AES data to compile these statistics. The data collected for each sample showed a predominance of Cu/(In+Ga) ratios that decrease at the GB. For each sample, the average Cu to group III ratio was calculated at the GI and at the GB. For the sample with a nominal Cu/(In+Ga) ratio of 0.78, the value of this ratio was 0.085 lower at the GB compared to the GI. The other three samples with Cu/(In+Ga) ratios of 0.85, 0.93, and 0.99 showed de-

creases of 0.024, 0.071, and 0.041, respectively. The samples with the largest number of scans performed also showed the largest average difference from GB to GI. The standard errors in the statistics for the GI values of the 0.78, 0.85, 0.93, and 0.99 composition samples were 0.011, 0.016, 0.011, and 0.014, respectively. The standard errors of the GB statistics were 0.022, 0.028, 0.029, and 0.022, respectively. Thus, in all but the 0.85 concentration sample the average differences are outside the statistical errors. In general, the observed Cu/(In+Ga) ratios were on the average approximately 30% lower than expected from the nominal value. This effect may be explained by the fact that some grains cleave along their boundaries rather than through the bulk of the grain. Our cleaves can expose both grain interiors and grain boundaries since cleaving can break apart grains as well as separate whole grains from each other. AES measurements across exposed grains would therefore not show significant changes between grain “interior” and grain boundary since both are actually boundaries. This is consistent with some of the minor AES variations already mentioned and the high surface sensitivity of the AES technique. However, many grains studied did show values close to the expected stoichiometry. From the statistical data, it was therefore possible to conclude that both types of grains were present after a cleave, with boundary-cleaved grains somewhat more common than bulk-cleaved grains. The average values listed above include all grains. In cases for which it appeared that the grain cleaved through its interior, the compositional changes are much larger than these averages, as shown in Fig. 1. Despite this, even grains with the low Cu/(In+Ga) ratios still displayed Cu deficiency at GBs. This is likely because the electron beam incident on the grain boundary probes proportionally more boundary versus interior volume. Similar analysis was performed for the O and Se species to test the predictions of Cahen and Noufi.⁶ The resulting data revealed no clear indication of increased O or decreased Se at GBs.

B. Secondary electron threshold

SET data from several samples showed pronounced work function decreases at GBs. Values of the work function difference between the semiconductor and the electron analyzer were determined from the onset energy of the SE emission, obtained from a linear extrapolation to the base line. We found that the accuracy of SET as a probe of gauging the work function is strongly dependent on both the level of surface contamination and the quality of the cleave. High amounts of contamination and a rough surface seem to suppress the SET onset from the CIGS layer in favor of onsets from contamination species and/or the Mo back contact. In order to determine the effects of a rough surface morphology on the SET measurement, the angular dependence of the SET peak was measured on a piece of gold foil, presputtered to remove contamination. We observed a relatively weak (less than 20 meV) dependence of the onset position for small ($<5^\circ$) angular changes relative to the surface normal. Somewhat larger (up to 200 meV) changes occurred as the angular variation reached 15° and rapidly progressed with changes in

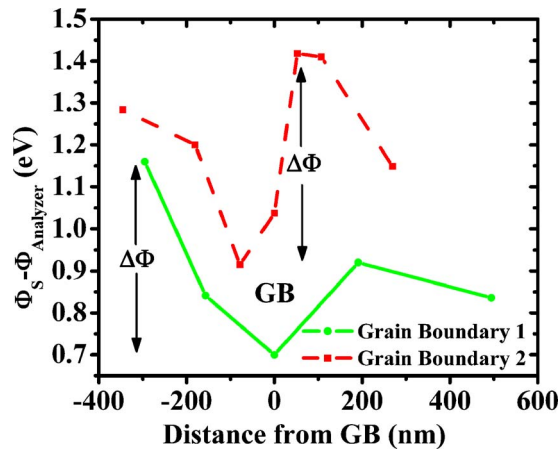


FIG. 2. Secondary electron threshold plotted vs position. Decreases occur at the GB for both data sets.

both the onset energy and intensity for angles $>20^\circ$. To avoid spurious onset changes due to uneven grain interfaces, care was taken to examine flat GBs with flat interfaces at normal incidence.

Figure 2 shows scans through two different GBs of the sample with nominal Cu/(In+Ga) ratio of 0.99. The work function difference between the sample and the analyzer (ΔE) is plotted for two separate runs versus distance from each GB. Negative distances indicate initial measurements in one grain, origin at the GB, and positive distances from the boundary into an adjacent grain. This figure shows decreases in the work function from 250 to almost 500 meV for grain boundaries 1 and 2, respectively. Other grain boundaries show similar decreases although such decreases can vary widely from $0 < \Delta\phi < 500$ meV. The error in these measurements is typically tens of meV with outliers $\leq \sim 200$ meV. These decreases in potential are qualitatively similar to the scanning Kelvin probe measurements of the band offsets at chalcopyrite GBs reported in Refs. 15 and 16, where the authors found a potential decrease (downward band bending) at the GBs of 100–200 meV, which is significantly less than the changes reported here. This indicates the importance of UHV in avoiding contamination not only for chemical composition analysis but also to correctly gauge potential changes.

C. Cathodoluminescence spectroscopy

CLS results were obtained for the sample with the nominal bulk Cu/(In+Ga) ratio of 0.99. This particular sample was cleaved *ex situ* and then immediately loaded into the vacuum chamber. The data was acquired through imaging of emission at particular wavelengths and through spectra collected from spots and rastered areas. Location-specific variations in CLS data were observed as well. Practically all the spectra exhibited multiple peaks, the positions of which vary from grain to grain. Figure 3 shows an example of several spectra taken from different regions of the sample: three distinct peaks with emission energies of 1.12, 1.16, and 1.19 eV are present in the spectra. Those features change in intensity

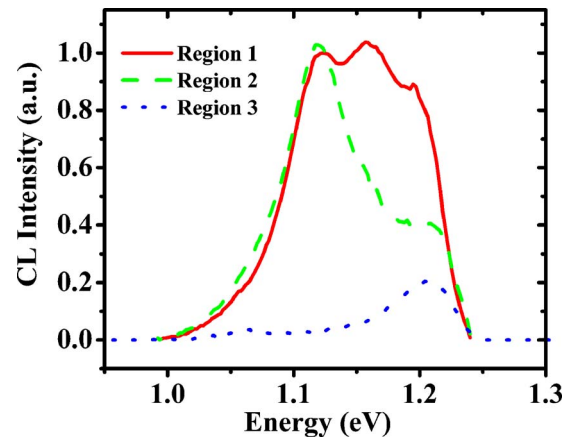


FIG. 3. CLS scans taken at 15 K from different regions of the sample with Cu/(In+Ga)=0.99 showing three distinct emission peaks whose relative peak intensities display pronounced spatial variation.

at different locations on the sample. The low energy tail on the spectra likely arises from defects and disorder within the film.²¹

CLS imaging at different fixed emission energies further illustrates this lack of uniformity. Figure 4 shows several CLS images superimposed on a corresponding SE image. The higher energy peaks are localized consistently near the back Mo contact while the lower energy peaks appear towards the surface of the sample. We also acquired point-by-point CLS measurements across a GB using the focused electron beam. Figure 5 shows three spectra taken at points in two adjacent GIs and at their corresponding GB. Little change is evident between the GB spectrum and the GI spectra.

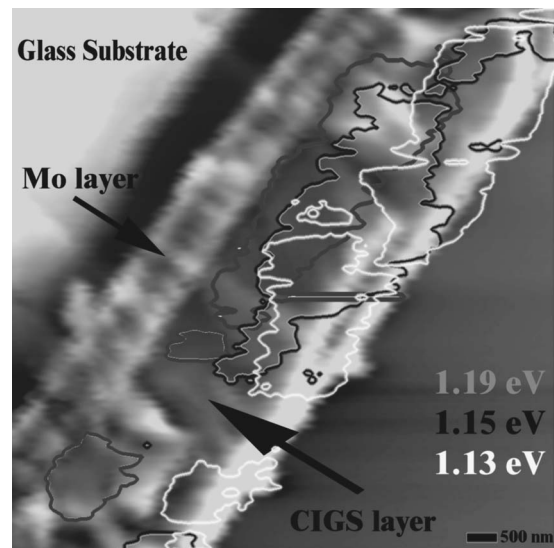


FIG. 4. CL maps performed at 15 K for three different energies (1.19, 1.15, and 1.13 eV), overlaid on the corresponding SEM image.

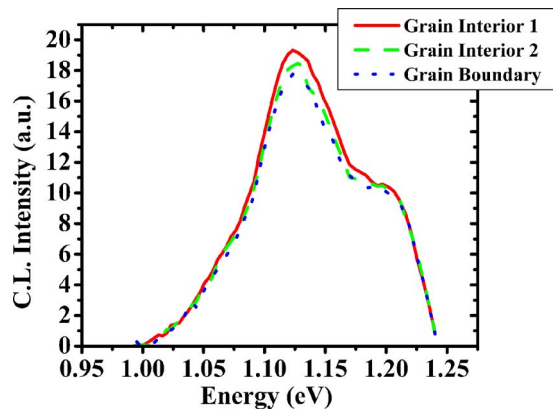


FIG. 5. CLS scans from within a GI, at an adjacent GI, and at their common GB showing no clear changes.

D. Secondary ion mass spectrometry

A SIMS depth profile for the sample with $\text{Cu}/(\text{In}+\text{Ga})$ equal to 0.99 is shown in Fig. 6. The data indicate a Ga gradient throughout the sample consistent with standard growth conditions¹ and the spatial dependence of the CLS results. The Ga signal drops by approximately 50% of its maximum value near the front surface of the film. A Na increase of over an order of magnitude (from approximately 10 to 200 counts \pm 10 counts) near the Mo back contact is typical and may be due to microstructure changes in the Mo surface. It is consistent with previously reported results.²² The depth profile also shows diffusion of In and Ga into the Mo layer, broadening the back interface. Imaging of the In and Ga signals within this broadened interface shows inhomogeneity in both the In and Ga signals laterally on a scale of tens of microns, much larger than the measurement resolution (120 nm), the typical grain size ($\sim 1 \mu\text{m}$), or the Mo layer roughness (90 Å). No lateral spatial localization of the Na signal was discernable either within the bulk CIGS layer or within the Mo layer.

IV. DISCUSSION

The AES results found for the CIGS specimens measured are consistent with theoretical predictions of Cu deficiency at

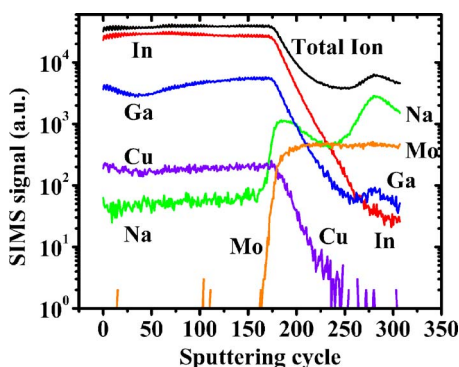


FIG. 6. SIMS depth profile through the CIGS film into the Mo back contact showing a Na pileup and interdiffusion at the CIGS-Mo interface. This data was taken from a $25 \times 25 \mu\text{m}^2$ area on the sample.

CIGS GBs.³ Indeed, the 25%–50% decreases of Cu content we observe experimentally are in good quantitative agreement with those predicted by Jaffe and Zunger.¹⁰ While the exact interfacial characteristics of the chemical bonding at GBs are not known, models that assume GBs to be similar to free surfaces are reasonable since neighboring grains may not form chemical bonds between them. GBs are commonly modeled as back to back Schottky barriers, and this is consistent with an approach assuming the GBs to be similar in character to free surfaces. There are several factors that could explain the lateral spread in our AES data in light of the predictions of Ref. 3. First, some of the grain-to-grain variation is due to the fact that not all the GBs probed are terminated by the polar surfaces calculated theoretically. Also, real GBs will not have a uniform spatial gap between them, nor is it necessary that real GBs be terminated by a single row of charge-neutralizing vacancies. In reality, the distribution of Cu is likely to be much more complicated with some spatial extent away from the GBs. This could be related to the formation of an extended ordered defect compound mentioned in Ref. 3. The beam spreading noted above also contributes to the apparent lateral spreading. SET measurements indicating a 200–400 meV lowering of the work function at the GBs are also in close agreement with Persson and Zunger's theory suggesting a similar decrease in the valence band maximum due to Cu deficiency.³ These phenomena may explain the superior performance of polycrystalline versus single crystalline CIGS-based² devices as follows.³ Recombination at the GBs is reduced since the lower valence band energy repels majority carrier holes from GB recombination sites. GBs themselves may serve to reduce overall defect density since they may getter defects. By contrast, the defect distribution in single crystals is rather uniform with the average values possibly greater due to the absence of gettering mechanisms. As mentioned earlier, we found no detectable change in either the Se or O signals at the GBs. It should be noted, however, that the AES detection limit for changes in surface Se or O composition as described in Ref. 6 is at the percent level, whereas concentration changes at the 0.1% level could produce significant (~ 0.1 eV) changes in band bending.

The 0.2–0.4 eV lower valence band calculated for the GB in Ref. 3 represents a band offset with the GB valence band maximum below the GI valence band maximum. Our experimental values for the decrease of the work function at GBs relative to GIs often measured several hundred meV, indicating the bending of the vacuum level down from the bulk to the boundary.

It should be emphasized that such conclusions were reached despite substantial inhomogeneity overall. Indeed, grain-to-grain variations produced substantial deviations from the average. Therefore, it was important to perform measurements and analysis on a grain boundary-by-grain boundary basis in order to elucidate the microscopic properties of polycrystalline CIGS. In addition, the accumulation of

relevant statistics on the CIGS layer properties required a large number of measurements across various regions of the samples.

The observed SET inhomogeneities were stronger than those exhibited in the AES and CLS measurements. Sometimes grain-to-grain potential changes were so significant that they obscured any changes of potential at the GBs. We attributed these observations to several factors: (i) variations in grain-to-grain stoichiometry, (ii) potential differences between grain facets with dissimilar crystallographic orientations (consistent with the reported Kelvin probe results²³), and (iii) variations in cleavage—grain surface versus grain bulk—described above.

Figure 3 shows significant nonuniformity in the CLS spectra of the different emission features. One possible explanation for this is variation in group I to group III composition. Indeed, our AES results indicate substantial grain-to-grain differences in Cu/(In+Ga) stoichiometry. A strong dependence of the emission spectra on the group I to group III composition ratio has been reported previously.^{24,25} In addition, the observed CLS nonuniformity may be associated with the considerable grain-to-grain variation in the In/Ga ratio, which we also observed in our Auger experiments. Such a variation would have an impact on the CL spectra because of the increasing band gap with increasing Ga content.²⁶ In fact, there is also a gradient of Ga decreasing away from the CIGS/Mo interface, as seen from the SIMS depth profiles. This gradient is an intentional feature of the solar cell growth process.¹ Matching this gradient, CLS images show a predominance of higher-energy CLS emission peaks in the vicinity of the same interface.

The nature of the CL near band edge (NBE) emission features remains an open question. Commonly, the NBE luminescence in CIGS has been attributed to excitonic and donor-acceptor pair recombination (See, for example, Refs. 24 and 27). Recently, an alternative model has been suggested¹⁷ in which radiative recombination in CIGS was explained employing a concept of quasi-donor-acceptor pair^{25,28} (qDAP) transitions. qDAP luminescence arises in materials with high concentrations of compensated stoichiometric defects. The qDAP emission intensity exhibits a distinctive dependence on both temperature and the power of excitation. Romero *et al.*¹⁷ reported results supporting a qDAP model for plan-view low-temperature micro-CL performed on samples similar to those used in our study. In our experiments, we employed low-temperature micro-CL on a cleaved cross section (see Fig. 4) and found both the positions and the distribution of the emission features to be substantially different from those reported in Ref. 17. Our low-temperature photoluminescence experiments (not shown) did not yield a positive confirmation of the qDAP nature of the transitions observed. One possible explanation for differences between our results and those reported in Ref. 17 may be the experimental geometry—normal to the growth direction here versus normal to the growth plane in Ref. 17. One may expect the luminescent properties of the free surface of CIGS films to be quite different from those of the bulk since

this surface is known to have considerable variations in stoichiometry.^{21,29} Additionally, the discrepancy between our CL results and those of Ref. 17 can be attributed to their surface versus our interior cleaved specimens, given the known changes in chemical and electronic properties that can occur with extended air exposure.

CLS spectra taken in the vicinity of GB (Fig. 5) show little change between GB and GI. Notwithstanding the substantial chemical and electronic changes we obtained from AES and SET measurements, our data exhibits no evidence of the wider band gap predicted at the GBs. However, a wider gap may yet be present since the excited electron-hole pairs generated at the GBs are likely to diffuse away from any higher band gap region before recombining. This effect is commonly observed in optoelectronics where wider gap “windows” are used to avoid recombination at surfaces of narrower gap semiconductors.³⁰ This effect is also evident in previous CLS studies where free carriers within a diffusion length of a quantum well recombine in the lower gap.³¹ We are pursuing alternative spectroscopy approaches to gauge such band gap changes near GBs. The absence of major changes in CLS features between grains and their boundaries is presented here for completeness.

The broadening of the In and Ga SIMS depth profile at the Mo back interface could be explained by the Mo surface roughness or interdiffusion. The Na SIMS signal detectable within the CIGS layer, which increases gradually toward the Mo layer, corresponds to concentrations not exceeding 1%, since our AES experiments did not yield any detectable Na peaks. We cannot draw any conclusions from our results regarding Na contribution to the solar cell performance. Our AES spectra indicated Cu/(In+Ga) nominally 30% below that expected, although this may simply reflect a CIGS-matrix variation in elemental sensitivity factors. Our SIMS measurements are only relative in the absence of standards. O concentrations for the samples were not available with our O sputter beam.

AES, SET, CLS, and SIMS measurements with submicron resolutions performed on solar-cell grade CIGS polycrystalline samples revealed the reduction of Cu content at GBs and related variation of the work function. These observations were achieved despite a significant compositional and optoelectronic nonuniformity throughout the CIGS layers. The elucidation of a relationship between work function changes and GB stoichiometry will require additional experimental efforts, which would have to relate, e.g., SET onsets with AES core level positions. Nanoscale AES/SET/CLS studies of the influence of the Ga/In ratio as well as oxidation and material aging could be important for better understanding and control of photovoltaic performance of chalcopyrite materials.

V. CONCLUSIONS

Polycrystalline CIGS exemplifies a material system in which high near-surface defect concentrations may be beneficial. Our results confirm theoretical predictions of a major decrease in Cu composition at grain boundaries. The Cu-

depleted GB interfaces can inhibit hole recombination, generating higher photocurrents. Our results show that the vacuum level relative to the Fermi level decreases substantially near the GBs, consistent with either a band offset due to Cu vacancy formation or *p*-type band bending. In either case, the hole barrier that forms serves to inhibit majority carrier movement away from the GBs and therefore reduces recombination. We found major nonuniform grain-to-grain stoichiometry, which can account for the well known difficulty maintaining CIGS uniformity in device structures. Our report emphasizes the importance of studying such complex systems as polycrystalline CIGS employing nanoscale resolution, UHV environment, and careful sample preparation procedures.

ACKNOWLEDGMENTS

This work was supported by DOE Grant No. DE-FG02-97ER45666 (localized AES and CLS, Jane Zhu). Two of the authors (M.A.C. and A.Z.) are supported by DOE-EERE under NREL Grant No. DEAC36-98-G010337. The authors would like to thank Markus Gloeckler for useful discussions.

¹K. Ramanathan *et al.*, Prog. Photovoltaics **11**, 225 (2003).

²A. Rockett, A. Agarwal, L.-C. Yang, E. Banda, G. Kenshole, C. J. Kiely, and H. Talich, *Proceedings of the 21st IEEE Photovoltaic Specialists Conference* (IEEE, New York, 1990), p. 764.

³C. Persson and A. Zunger, Phys. Rev. Lett. **91**, 266401 (2003).

⁴S. Schuler, S. Nishiwaki, J. Beckmann, N. Rega, S. Brehme, S. Siebentritt, and M. C. Lux-Steiner, *Proceedings of the 29th IEEE Photovoltaic Specialist Conference* (IEEE, New York, 2002), p. 504.

⁵M. Gloeckler, J. R. Sites, and W. Metzger, J. Appl. Phys. **98**, 113704 (2005).

⁶D. Cahen and R. Noufi, Appl. Phys. Lett. **54**, 558 (1989).

⁷L. Kronik, U. Rau, J.-F. Guillemoles, D. Braunger, H. W. Schock, and D. Cahen, Thin Solid Films **361–362**, 353 (2000).

⁸R. J. Matson, L. L. Kazmerski, R. Noufi, and D. Cahen, J. Vac. Sci. Technol. A **7**, 230 (1989).

⁹N. Moll, A. Kley, E. Pehlke, and M. Schaffer, Phys. Rev. B **54**, 8844 (1996).

¹⁰J. E. Jaffe and A. Zunger, Phys. Rev. B **64**, 241304(R) (2001).

¹¹D. Schmid, M. Ruckh, F. Grunwald, and H. W. Schock, J. Appl. Phys. **73**, 2902 (1993).

¹²S. H. Wei and A. Zunger, J. Appl. Phys. **78**, 3846 (1995).

¹³I. Visoly-Fisher, S. R. Cohen, A. Ruzin, and D. Cahen, Adv. Mater. (Weinheim, Ger.) **16**, 879 (2004).

¹⁴M. A. Contreras *et al.*, *Proceedings of the First WCPEC/24th IEEE Photovoltaic Specialist Conference* (IEEE, New York, 1994), p. 68.

¹⁵Ch. Sommerhalter, S. Sadewasser, Th. Glatzel, Th. W. Matthes, A. Jäger-Waldau, and M. Ch. Lux-Steiner, Surf. Sci. **482–485**, 1362 (2001).

¹⁶C.-S. Jiang, R. Noufi, J. A. AbuShama, K. Ramanathan, H. R. Moutinho, J. Pankow, and M. M. Al-Jassim, Appl. Phys. Lett. **84**, 3477 (2004).

¹⁷M. J. Romero, K. Ramanathan, M. A. Contreras, M. M. Al-Jassim, R. Noufi, and P. Sheldon, Appl. Phys. Lett. **83**, 4770 (2003).

¹⁸M. J. Hetzer, Y. M. Strzhemechny, M. Gao, M. A. Contreras, A. Zunger, and L. J. Brillson, Appl. Phys. Lett. **86**, 162105 (2005).

¹⁹X. L. Sun, L. J. Brillson, Y.-M. Chiang, and J. Luo, J. Appl. Phys. **92**, 5072 (2002); X. L. Sun, S. H. Goss, L. J. Brillson, D. C. Look, and R. J. Molnar, *ibid.* **91**, 6729 (2002).

²⁰C. J. Powell, Appl. Surf. Sci. **230**, 327 (2004).

²¹Y. M. Strzhemechny, P. E. Smith, S. T. Bradley, D. X. Liao, A. A. Rockett, K. Ramanathan, and L. J. Brillson, J. Vac. Sci. Technol. B **20**, 2441 (2002), and references therein.

²²A. Rockett, J. S. Britt, T. Gillespie, C. Marshall, M. M. Al-Jassim, F. Hasoon, R. Matson, and B. Basol, Thin Solid Films **372**, 212 (2000).

²³S. Sadewasser, Th. Glatzel, M. Rusu, A. Jäger-Waldau, and M. Ch. Lux-Steiner, Appl. Phys. Lett. **80**, 2979 (2002).

²⁴S. Zott, K. Leo, M. Ruckh, and H.-W. Schock, Appl. Phys. Lett. **68**, 1144 (1996).

²⁵A. Bauknecht, S. Siebentritt, J. Albert, and M. Ch. Lux-Steiner, J. Appl. Phys. **89**, 4391 (2001).

²⁶I. V. Bodnar, A. P. Bologa, and B. V. Korzun, Phys. Status Solidi B **105**, K31 (1982).

²⁷A. Rockett and R. W. Birkmire, J. Appl. Phys. **70**, R81 (1991).

²⁸B. I. Shklovskii and A. L. Efros, *Electronic Properties of Doped Semiconductors* (Springer, Berlin, 1984).

²⁹D. Liao and A. Rockett, Appl. Phys. Lett. **82**, 2829 (2003).

³⁰P. Battacharya, *Semiconductor Optoelectronic Devices* (Prentice Hall, Upper Saddle River, NJ), p. 438.

³¹L. J. Brillson, T. M. Levin, G. H. Jessen, and F. A. Ponce, Appl. Phys. Lett. **75**, 3835 (1999).